Corrosion Science 53 (2011) 2233–2246

Contents lists available at ScienceDirect

Corrosion Science

journal homepage: www.elsevier.com/locate/corsci

An ESEM *in situ* investigation of initial stages of the KCl induced high temperature corrosion of a Fe–2.25Cr–1Mo steel at 400 °C

T. Jonsson [a,*], N. Folkeson [a], J.-E. Svensson [a], L.-G. Johansson [a], M. Halvarsson [b]

[a] Department of Chemical and Biological Engineering, High Temperature Corrosion Centre, Chalmers University of Technology, SE-412 96 Göteborg, Sweden
[b] Department of Applied Physics, Chalmers University of Technology, SE-412 96 Göteborg, Sweden

ARTICLE INFO

Article history:
Received 17 May 2010
Accepted 11 March 2011
Available online 21 March 2011

Keywords:
A. Low alloy steel
B. SEM
B. XRD
C. High temperature corrosion
C. Chlorination

ABSTRACT

The initial oxidation of a low-alloyed steel (Fe–2.25Cr–1Mo) in the presence of small amounts of KCl(s) have been investigated through ESEM *in situ* exposure and analysis at 400 °C. The samples were also characterized by XRD, SEM/EDX and FIB. The present study shows the corrosive nature of KCl towards the low alloyed steel. It is concluded that the initial KCl distribution is important and that a $KCl/FeCl_2$ liquid phase film forms on large parts of the oxide surface in the presence of KCl. It is proposed that Cl increases the oxidation rate (by decorating oxide grain boundaries) and decreases the oxide scale adhesion.

1. Introduction

Low alloyed steels are frequently used in steam superheater tubes in power plants because of their low cost and excellent mechanical properties. At moderate temperatures, (<500 °C in mildly corrosive environments) low alloyed steels form an oxide scale consisting of hematite (Fe_2O_3) and magnetite (Fe_3O_4) which has sufficient protective properties for many applications. At higher temperature and in more corrosive environments the rate of oxidation becomes too great and the low alloyed steels are replaced by different types of stainless steels. The literature on the oxidation properties of low alloyed steels is summarized by Kofstad [1] and Birks and Meier [2]. The corrosivity of the fireside environment in a boiler is strongly dependent on fuel composition. Thus, power boilers firing household waste feature much more aggressive fireside environments compared to a boiler firing coal. Recently, power boilers firing different types of biomass have also reported considerable problems with superheater corrosion [3]. Actually, the maximum steam temperature in boilers firing household waste and biomass is reported to be limited by fireside corrosion [3]. The high corrosivity in biomass- and waste-fired boilers has been attributed partly to the presence of high levels of alkali chlorides (NaCl and KCl) in the flue gas [4,5].

Many authors attribute the corrosiveness of alkali chlorides towards high temperature steels primarily to the chlorine component and a mechanism called "active oxidation" has been suggested to explain the results [5–11]. Other authors consider that the formation of low melting salt mixtures is essential (e.g. $KCl/ZnCl_2$) [12]. Several recent studies report on the high temperature corrosion effects of potassium salts in the presence of O_2 towards stainless steels [13–18]. It was shown that the potassium ion plays an important role in initiating corrosion by reacting with the protective oxide and depleting it in chromium [16–18]. The alkali chloride-induced corrosion of stainless steels is reported to be very fast initially [16–18].

A recent study has shown that KCl is quite corrosive towards the low-alloyed steel Fe–2.25Cr–1Mo at 400 °C [19], the initial reaction being very fast. Because the initial stages of corrosion are considered to strongly influence the later corrosion behaviour, it is useful to study the early stages of the KCl-induced corrosion of this material. *In situ* exposure and analysis, within the environmental scanning electron microscope (ESEM) sample chamber, are powerful tools to do this. The advantages of the ESEM *in situ* exposure technique have been reported [20–22]. Monitoring the formation of corrosion products *in situ* can provide unique information on corrosion mechanisms. Oxidation of iron at 500 °C in dry and wet air was recently studied by the ESEM *in situ* technique [23]. That study compared the microstructure and composition of oxide scales formed under ESEM *in situ* exposure with corresponding oxide scales formed in well-controlled exposures at atmospheric pressure. The agreement was excellent, confirming the suitability of the *in situ* exposure technique to study these iron oxide-forming steels. To provide a better understanding of corrosion mechanisms it is important to complement the *in situ* exposure with additional information on the microstructure of the

* Corresponding author.
E-mail address: tj@chalmers.se (T. Jonsson).

0010-938X/$ - see front matter © 2011 Elsevier Ltd. All rights reserved.
doi:10.1016/j.corsci.2011.03.007

corroded surface. Focused ion beam (FIB) milling and imaging in combination with analytical scanning electron microscopy with energy dispersive X-ray (SEM/EDX) are excellent methods to do this. The FIB technique gives the possibility to produce cross-sections of selected features with high accuracy. To follow the corrosion process on a specific part of the surface *in situ* in the ESEM and then study the microstructure of the same region in detail by FIB and SEM/EDX can provide more insight into the corrosion mechanisms. The aim of this work is to use this unique combination of tools to elucidate the initial stages of corrosion of Fe–2.25Cr–1Mo in the presence of small amounts of KCl at 400 °C.

2. Experimental

2.1. Experimental strategy

In order to be able to study the initial corrosion mechanisms on Fe–2.25Cr–1Mo in the presence of small levels of KCl(s) the ESEM *in situ* exposure technique can been used. However, the possibility to study the oxidation process live, *in situ*, on specific locations on the sample puts high demand on pre-exposure analysis. In order to meet this demand special effort was made to characterize the starting condition, e.g. salt distribution. The samples were therefore marked so that the exact positions could be found in the different microscopes and analyzed before, during and after exposure. Section 2 is based on this experimental approach divided into four parts: sample preparation, pre-exposure analysis, exposure analysis and post-exposure analysis.

Some of the corrosion products (i.e. metal chlorides) formed in the presence of KCl at 400 °C are expected to be unstable at room temperature in humid air. In order to minimize the influence of sample storage on these unstable corrosion products the exposures, sample preparation and analysis were performed in one sequence and transportation between the microscopes were done in desiccators over P_2O_5. The results were also compared with the results from a furnace study of KCl on Fe–2.25Cr–1Mo [19]. In order to be able to make this important comparison the same methods regarding polishing and salt deposition were used as in [19].

2.2. Sample preparation and material

Metal coupons with dimensions $4 \times 4 \times 2\ mm^3$ were used for the ESEM *in situ* exposures. Larger samples ($15 \times 15 \times 2\ mm^3$) were ground to 320 grit on SiC and polished with 1 μm diamond suspension until the surface was mirror-like. The samples were then cut to their final size by cutting with a low speed saw. After cutting, the samples were cleaned and degreased in ethanol and acetone during ultrasonic agitation. KCl was applied by spraying the samples with a saturated solution of KCl in water/ethanol (20:80). The samples were dried with cool air and stored in a desiccator prior to exposure. Table 1 shows the chemical composition of the steel.

2.3. Pre-exposure analysis

A Leo Ultra 55 scanning electron microscope (SEM) was used to image the starting conditions before the ESEM *in situ* exposure. The SEM has a field emission electron gun (FEG) and is equipped with an in-lens secondary electron (SE) detector suitable for imaging at low accelerating voltages. The corners of the samples were first marked with a sharp pin in order to be able to image the same region in the different microscopes. Several KCl(s) particles together with a larger region around each particle were carefully investigated before each exposure and then followed *in situ* in the ESEM at temperature and analysed after the exposure. The exact starting condition could then be coupled to the formation of corrosion products during exposure and their composition (plan view and cross-section) after exposure.

Table 1
Elemental composition of Fe–2.25Cr–1Mo.

Element	Fe	Cr	Mo	Mn	Si	C	P	S
wt.%	96.01	2.19	0.93	0.49	0.26	0.095	0.014	0.01

2.4. Exposure analysis

Exposures and microscopy of the oxide scales were carried out *in situ* at 400 °C using an FEI Quanta 200 FEG ESEM in low vacuum (2.5 Torr), secondary electron mode. The ESEM has a field emission electron gun (FEG) and is equipped with a temperature control unit together with a heating stage. The heating stage consists of a furnace and a thermocouple with a water-cooling system, which is mounted in the sample chamber. The temperature is ramped up to the desired temperature. In this work the ramp speed used was 10 °C/min (for a few samples, initially) and 50 °C/min (maximum ramp speed, used for the majority of the samples). The temperature ramp was performed in the exposure atmosphere, which was ambient air (containing about 1% H_2O).

For all imaging at high temperature an accelerating voltage of 20–25 kV was used together with a special heat and light insensitive secondary electron detector. Working with a low pressure in the sample chamber (as during exposures) will cause the formation of positive charged ions. These are formed by low energy secondary electrons (SEs) interacting with molecules in the sample chamber creating a cascade effect of the SE signal but also positively charged ions. Besides that oxygen will be consumed during the oxidation process, some of the positively charged ions will be attracted to the negatively charged sample surface and neutralise charging of the sample. In order to avoid contamination special sample holders were used for the exposures where KCl was present.

2.5. Post-exposure analysis

2.5.1. X-ray diffraction (XRD)

Crystalline corrosion products were analyzed by X-ray diffraction (XRD) using a Siemens D5000 powder diffractometer, equipped with grazing incidence beam attachment and a Göbel mirror. Cu Kα radiation was used and the angle of incidence was 5°. The detector measured between $14° < 2\theta < 67°$.

2.5.2. Analytical scanning electron microscope (SEM/EDX)

After the *in situ* exposure the corrosion products were examined with an FEI Quanta 200 FEG ESEM both for plan view investigations and to investigate ion milled cross-sections (see below). The SEM has a field emission electron gun (FEG) and is equipped with Oxford Inca energy dispersive X-ray (EDX) system. SEM/EDX was used for elemental mapping and quantification with an acceleration voltage around 10 kV. The acceleration voltage was chosen in order to minimise the interaction volume within the sample but to still be able to use the K lines of Fe and Cr for a more accurate quantification.

2.5.3. Focused ion beam (FIB)/scanning electron microscope (SEM)

In order to prepare cross-sections of the corrosion products and the subjacent metal an FEI Strata DB 235M combined FIB/SEM system was used. It is a dual beam system, equipped with both an electron and ion column. The electron column is equipped with a FEG and the ion column with a liquid gallium source. The SEM column was used for general imaging and the FIB column was used for

cross-section preparation and imaging. In imaging mode the FIB works in a similar way as an SEM. Although the FIB uses gallium ions instead of electrons, the detected secondary electrons are transformed into an image in a similar way as in an SEM.

The samples were first investigated with the SEM column in order to select an interesting feature in the ESEM *in situ* analysed region of the sample. FIB milling was then performed in two steps to produce smooth cross-sections of the corrosion products and the subjacent metal. First, coarse milling was used to make a trench, i.e. a milled staircase into the underlying metal. Then the cross-section was polished using lower ion currents. During coarse FIB milling an accelerating voltage of 30 kV and high ion currents were used, 20 and 7 nA, and for the fine polishing lower currents were used typically 1 or 0.5 nA. The cross-sections were milled with 45° tilt relative to the sample surface through the features of interest. This made it possible to perform chemical analysis (SEM/EDX) of the ion milled cross-section by mounting the sample in the SEM with 45° tilt, i.e. 0° tilt of the cross-section normal.

3. Results

3.1. Reference exposures

3.1.1. Exposures in the absence of KCl

As a reference, polished Fe–2.25Cr–1Mo samples were subjected to ESEM *in situ* exposure in the absence of KCl for 60 min at 400 °C in air (2.5 Torr). The results showed a smooth featureless oxide scale covering the alloy surface. This is in good agreement with *ex situ* furnace exposures of Fe–2.25Cr–1Mo in O_2 at 400 °C, reporting a smooth thin iron-rich oxide scale to have formed after 60 min [24]. By inspection of ion milled cross-sections, scale thickness was measured to be 100–200 nm after the *in situ* exposure, in good agreement with the mass gains recorded in the furnace study.

3.1.2. Behaviour of KCl during in situ exposure conditions

The ESEM *in situ* exposures are performed at lower pressure than ordinary furnace exposures (2.5 Torr compared to about 760 Torr) and under the electron beam. This has previously been shown to not affect the oxidation of pure iron in dry and wet air at 500 °C [23]. Accordingly, the reference exposure resulted in an oxide morphology and oxide thickness in good agreement with the corresponding furnace exposures. To check the influence of the *in situ* exposure technique on the deposited salt particles, a gold surface with KCl particles was exposed *in situ* at 400 °C. No evidence was found for the electron beam having any effect on the morphology of the KCl crystallites. Gravimetry showed that about 20% of the deposited KCl had evaporated from the gold surface after 60 min exposure *in situ*. This may be compared to a corresponding experiment at 500 °C and atmospheric pressure where about 1% of the KCl had evaporated after 60 min.

3.2. Pre-exposure analysis

3.2.1. Distribution of KCl on the surface

The pre-exposure analysis of the salt sprayed samples showed a wide size distribution of KCl particles. This is in accordance with several previous studies [13–18]. During a furnace study of the behaviour of KCl on Fe–2.25Cr–1Mo at 400 °C, the largest KCl particles or clusters of particles (50–200 μm) remained mostly un-reacted after 60 min exposure while smaller particles were completely consumed and covered by corrosion products [19]. In the present *in situ* exposures, relatively small (10–20 μm) KCl particles were selected for study.

Using standard settings 20 kV accelerating voltage and the conventional Everhart–Thornley (ET) SE detector showed no evidence for the presence of KCl on the steel surface between the KCl particles. However, using an acceleration voltage of 2 kV together with the in-lens detector, as described in Section 2, enabled imaging of the KCl present in between the larger KCl particles, see e.g. Fig. 1b. This knowledge regarding the starting conditions proved invaluable for interpreting the initial corrosion process in the ESEM *in situ* analysis since it showed that the KCl particles could be divided into two types. Thus, some areas were dominated by isolated particles, i.e. particles not surrounded by observable amounts of KCl, (termed type a, see Fig. 1a) while other parts of the surface exhibited KCl particles surrounded by small amounts of tiny KCl

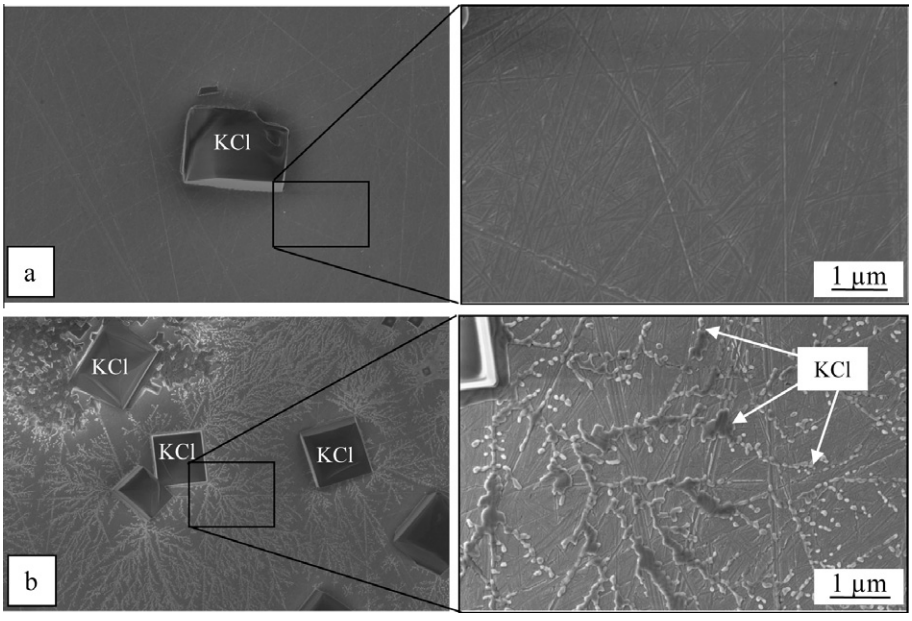

Fig. 1. SEM/SE images acquired with the in-lens detector at 2 kV before exposure. The KCl(s) distribution could be divided into two types. (a) Isolated KCl particles where the KCl particle is surrounded by a KCl-free metal surface. The image on the right hand shows the metal surface with higher magnification. (b) KCl particles where the particles are surrounded by a thin dendritic network of KCl (shown with higher magnification on the right hand side).

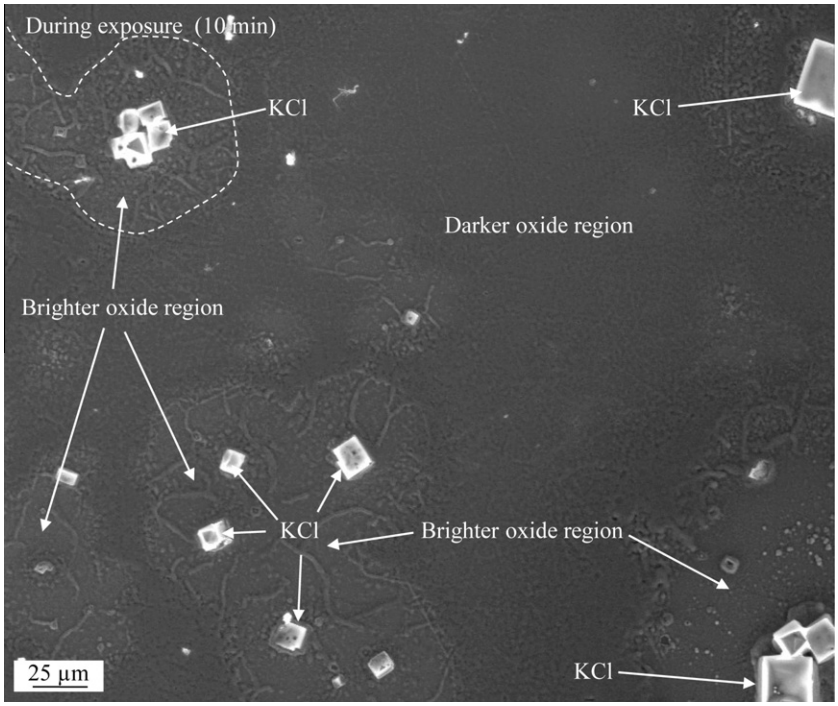

Fig. 2. Several isolated KCl particles are shown after 10 min ESEM *in situ* exposure at 400 °C. An about 10–30 μm wide, bright region around each isolated KCl particle appears to have a different surface morphology.

crystallites that form a dendritic pattern (termed type b, see Fig. 1b). It is suggested that the two different distributions of KCl on the surface is connected to the drying up of the salt solution droplets as they impinge on the surface.

3.3. Exposures with KCl

3.3.1. Isolated KCl particles (type a)

Fig. 2 shows a region containing several isolated KCl particles (type a) after 10 min *in situ* exposure. Around each KCl particle there is a 10–30 μm wide region with brighter contrast in the SE image (acquired at 400 °C). The appearance of the bright regions was not correlated to the size of the KCl particles and their extent did not change with exposure time. Tilt images after exposure and ion-milled cross-sections indicated that these regions typically have thinner oxide scale than the surrounding area.

Fig. 3a shows an isolated KCl particle (type a) at higher magnification before, during and after exposure. The "before exposure" image shows no sign of KCl dendrites in the vicinity of the KCl particle. The ESEM *in situ* images acquired after 17 and 35 min exposure show the formation of new oxide around the KCl particle, forming an oxide rim along its periphery. A comparison of the images acquired during and after exposure shows that the oxide rim grows with exposure time. The "after exposure" image was acquired at a 52° tilt and shows the KCl particle with its oxide rim. In accordance with the low magnification image in Fig. 2, the KCl particle is surrounded by an area with relatively thin oxide scale (marked region).

Fig. 3b shows an ion-milled cross-section (with 45° tilt) though the KCl particle in Fig. 3a. The KCl particle appears bright in the SE image. The cross-section reveals that the KCl particle has become hollow, consisting only of a thin shell. The oxide rim around the KCl particle is about 2 μm thick and 2 μm wide while the oxide scale beneath the partially consumed KCl particle is about 0.5 μm thick. The oxide rim and the scale beneath the partially consumed KCl particle both consist of iron-rich oxide. XRD showed the presence of spinel (M_3O_4) and KCl, in good agreement with the corrosion products detected after 1 h exposure in a furnace study [19]. Only low levels (<1 at.%) of K, Cl and Cr could be found in the oxide rim and in the upper part of the oxide scale.

The adhesion of the oxide scale was poor. The cross-section shows that the oxide is no longer attached to the metal substrate, leaving a gap between the oxide scale and the metal. No signs of spallation of the oxide scale were observed during any of the ESEM *in situ* exposures. Neither did the oxide microstructure indicate anything else than ion diffusion grown oxide scales. It is therefore suggested that the de-cohesion between scale and substrate has occurred during cooling. It is nevertheless difficult to exclude local spallation at the oxide/metal interface beneath the oxide scale at temperature.

3.3.2. KCl particles surrounded by KCl dendrites (type b)

3.3.2.1. Corrosion at the KCl particles. As noted above, part of the surface exhibited a thin network of KCl dendrites in between the KCl particles (Fig. 1b). Fig. 4a shows such a region before exposure at low magnification. The boxed area was imaged during the ESEM *in situ* exposure (Fig. 4b) and was also analysed after exposure (Figs. 4c–e). The *in situ* images (4b) show that oxidation starts already during temperature ramping (10°/min), see image acquired at 355 °C. The first oxide growth occurs mainly on the areas that appear bright before the reaction starts, at 330 °C. Oxide growth continues with increasing temperature and exposure time. With time, an oxide rim forms around the KCl particle, similar to that observed around the isolated KCl particles (type a) (see Figs. 2 and 3).

Simultaneous with the growth of the oxide rim, the KCl particle appears to be consumed, and a depression appears in its top surface, which was originally flat. With time, the KCl particle becomes completely overgrown by oxide (see images acquired at 400 °C 0, 2, 7 and 20 min). After 20 min of exposure at 400 °C the former KCl particle is completely covered with a thick oxide scale and the exposure was interrupted. This behaviour is typical of type b KCl particles (those originally surrounded by small amounts of KCl). The region shown in Figs. 4a and b is also depicted in the tilted

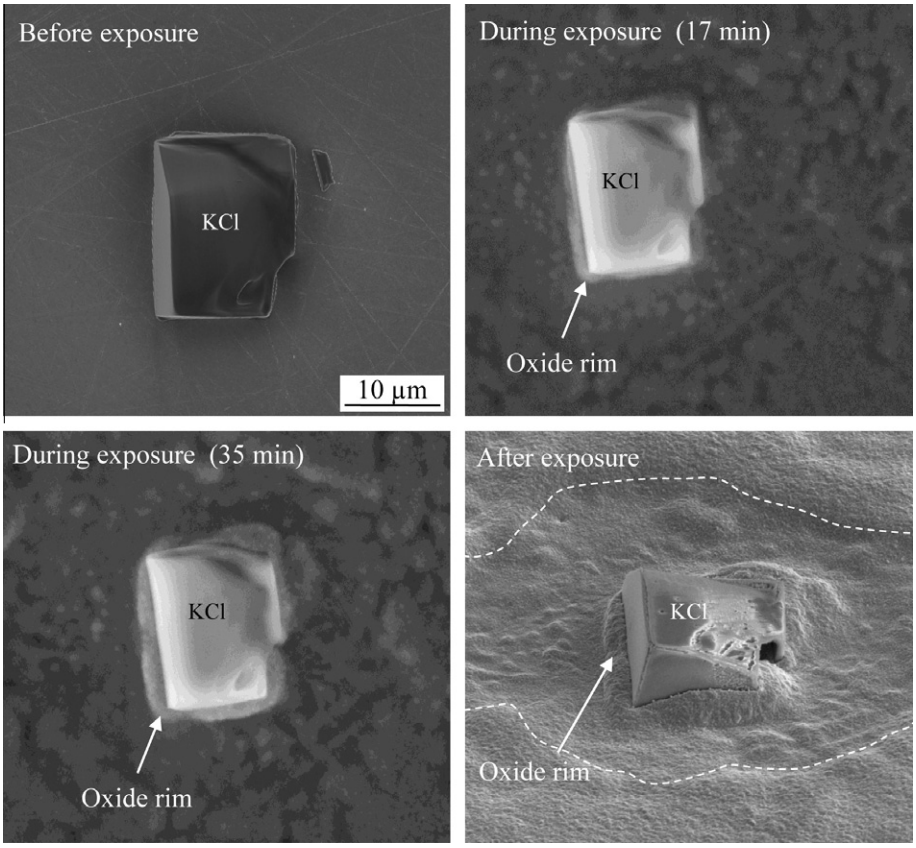

Fig. 3a. An isolated KCl particle is shown before exposure, during ESEM *in situ* exposure and after exposure. The oxide rim around the KCl particle was growing with exposure time. The after exposure SE image shows the particle with 52° tilt. The oxide rim surrounding the KCl particle can easily be seen in the tilt image as well a region with thinner oxide scale (marked region).

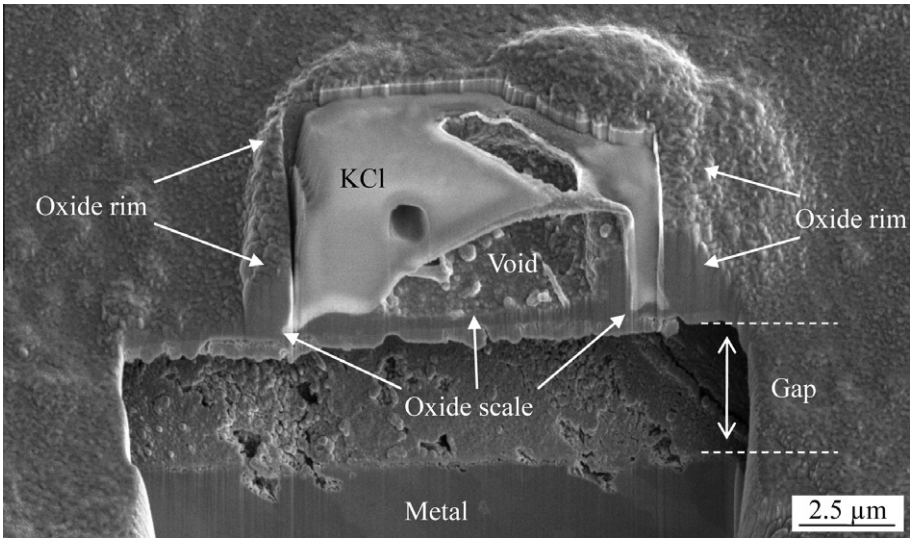

Fig. 3b. An ion-milled cross-section through the isolated KCl particle shown in Fig. 3a. The cross-section was milled with 45° tilt in order to be able to perform subsequent SEM/EDX analysis. The oxide rim around the KCl particle and a sub-micrometer thick oxide scale beneath the KCl particle can be seen. The KCl particle is hollow and the whole oxide scale has spalled from the metal.

SE image, showing the situation after 20 min exposure (Fig. 4c). While some KCl particles can still be seen at this stage, most KCl particles have now become completely overgrown by thick oxide. The corrosion process is appreciably faster than for the corresponding isolated KCl particle shown in Fig. 3a.

Fig. 4d shows a BSE image of the ion-milled cross-section indicated in Fig. 4c, i.e. cutting through the particle imaged in Figs. 4a–c before, during and after exposure. It may be noted that the KCl in the original particle is now completely consumed. The corrosion products at this position are situated both above and below the ori-

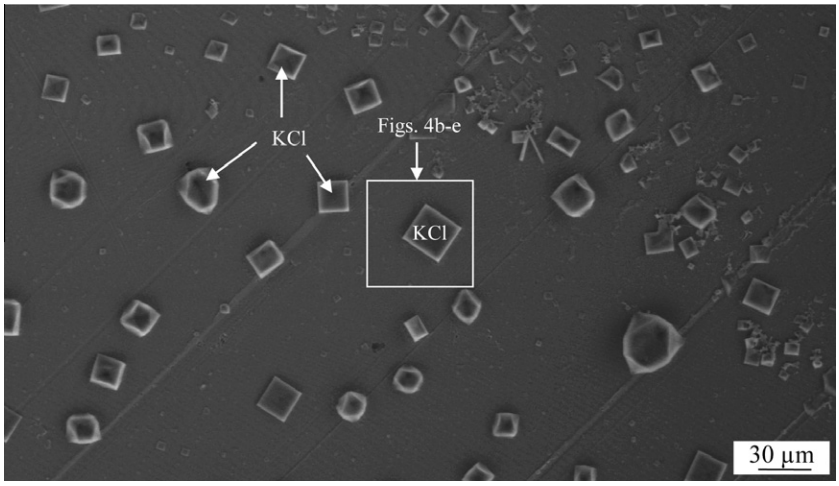

Fig. 4a. A region containing several KCl particles surrounded with a thin dendritic network pattern of KCl is shown before exposure with low magnification. The marked area is imaged during the ESEM *in situ* exposure and analysed after exposure, see Fig. 4b–e.

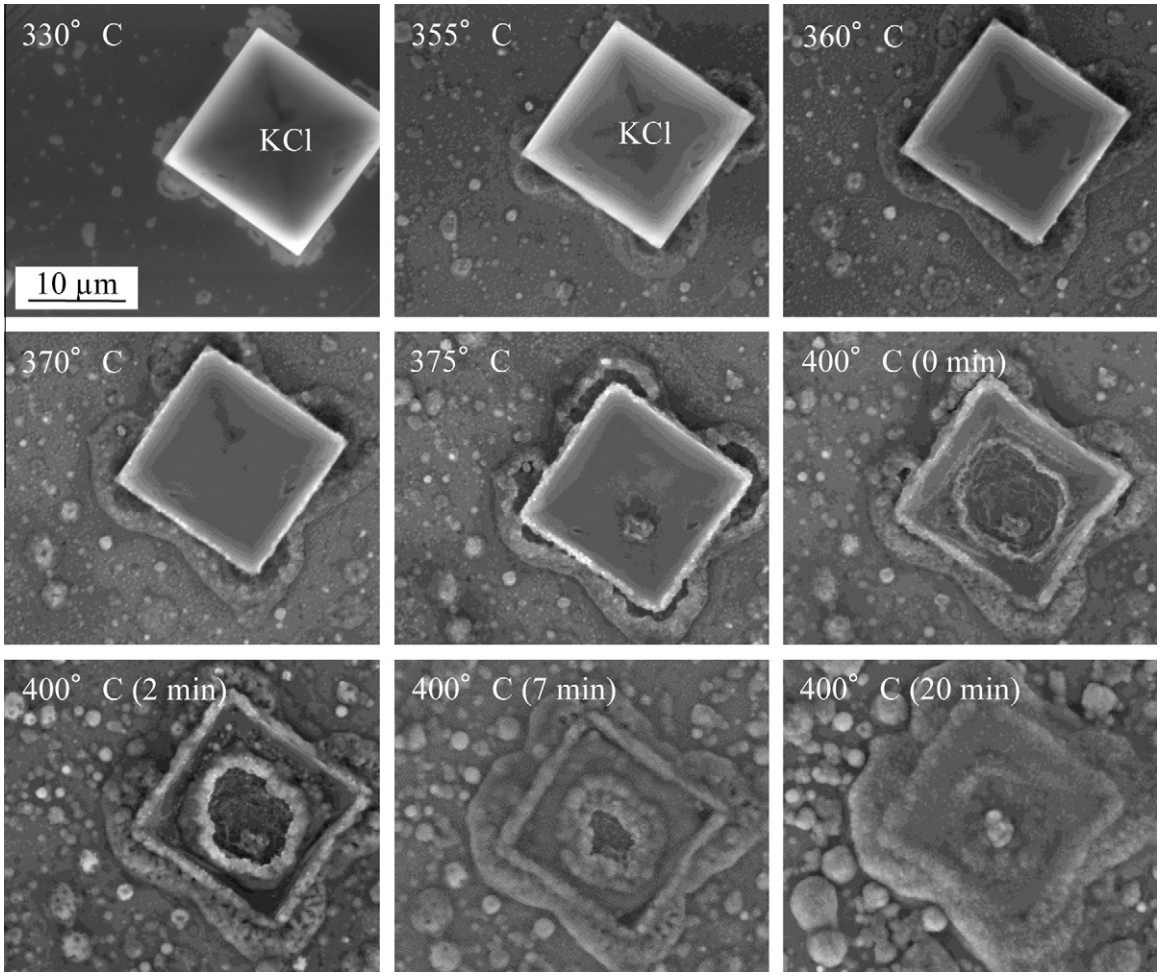

Fig. 4b. ESEM *in situ* image acquired during temperature ramping (10°/min) and during 20 min of exposure at 400 °C of a KCl particle surrounded with a thin dendritic network pattern of KCl (shown in Fig. 4a). The corrosion process starts already during temperature ramp (355 °C) and the whole KCl particle is consumed and overgrown with oxide after 20 min of exposure. The exposure was terminated after 20 min exposure. Fig. 4c and d show an after exposure images of the particle.

ginal metal surface (the hatched line in the image). The outermost layer is relatively dense, covering a porous region that corresponds to the position of the former KCl particle. Beneath the original metal surface the scale is porous. SEM/EDX maps of the cross-section (Fig. 4e) show that the scale above the original metal surface consists of iron-rich oxide. In contrast, the inner (inward growing) part of the scale contains large amounts of Cl together with Fe and O. SEM/EDX quantification confirms that the outer part of the oxide

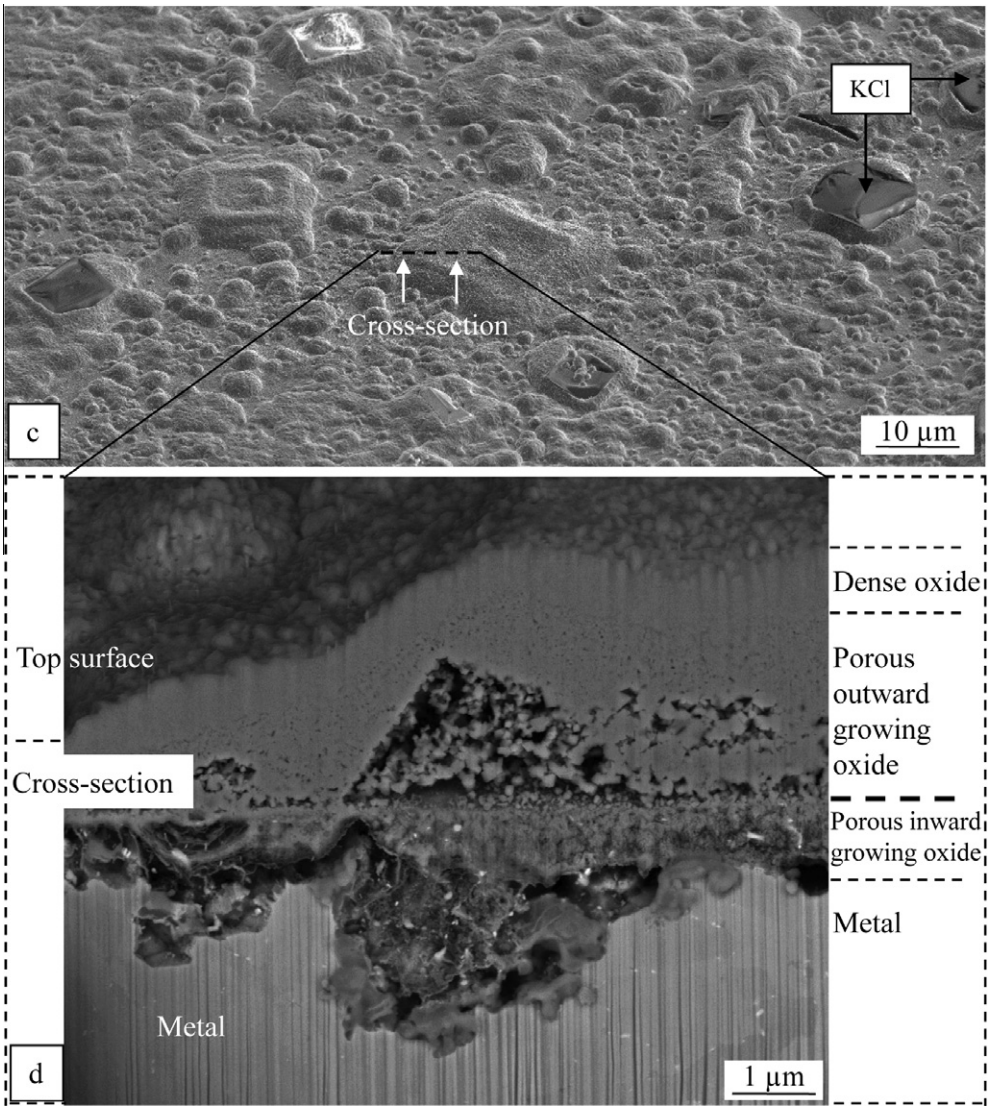

Fig. 4c and d. (c) An SE image of the sample exposed for 20 min. It shows the KCl particle surrounded with a thin dendritic network pattern of KCl (shown in Fig. 4a–b). The sample is tilted 52° showing the corrosion products after several former KCl particles together with some still KCl containing particles. (d) A BSE image of the ion-milled cross-section marked in (c). The cross-section was milled with 45° tilt in order to be able to acquire subsequent SEM/EDX analysis. The thick dashed line marks the original metal surface. SEM/EDX maps of the cross-section are shown in Fig. 4e.

scale consist of an iron-rich oxide (containing <1 at.% of K and Cl), while the inward growing part consists of a mixture of iron oxide and iron chloride (up to 10 at.% Cl). In addition, (1–4 at.%) Cr was present in the inward growing scale.

3.3.2.2. Corrosion between the KCl particles. The SE tilt image of the sample exposed for 20 min exposure (Fig. 4c) shows an uneven surface containing many oxide nodules in between the former KCl particles, showing that this part of the surface also suffered rapid corrosion. This behaviour was typical for these regions and was studied in detail.

Fig. 5a shows a region of the surface before exposure featuring type b KCl particles (surrounded by small amounts of KCl dendrites). The images show the evolution of the microstructure during and after the *in situ* exposure. Sub-micrometer spherical oxide nodules appear between the KCl particles after 10 min exposure (marked with arrows in the image). The location of the oxide nodules was not correlated to the KCl dendrites observed before exposure. After shorter exposure times there was no evidence for accelerated corrosion at the locations where nodules later developed. The oxide nodules grow with time and new nodules "nucleate" throughout the exposure, see images acquired after 10, 20, 30 and 50 min. Indeed, the size of the oxide nodules is correlated to the time of "nucleation", the youngest nodules being smallest. Fig. 5b is a SE image of the region shown in Fig. 5a (taken at 52° tilt angle) after 60 min exposure. The image illustrates the corrosion products formed on former type b KCl particles (square shaped) and the rounded oxide nodules in between (Fig. 5a). At this stage, some of the oxide nodules have reached about 4 µm in diameter. The position of an ion-milled cross-section through some of the oxide nodules is marked in the image and the corresponding BSE image is shown in Fig. 5c. The cross-section was milled with 30° tilt. SEM/EDX maps of the cross-section are shown in Fig. 5d. The cross-section shows that the oxide nodules are not correlated to localized corrosion of the metal substrate, there being no tendency for pit formation below the nodules. Also, the nodules tend to be hollow and often feature accumulations of KCl in their top parts (see the K and Cl maps in Fig. 5d). This was verified through sequential milling of several cross-sections, with imaging in between, through the oxide nodules, to give three-dimensional

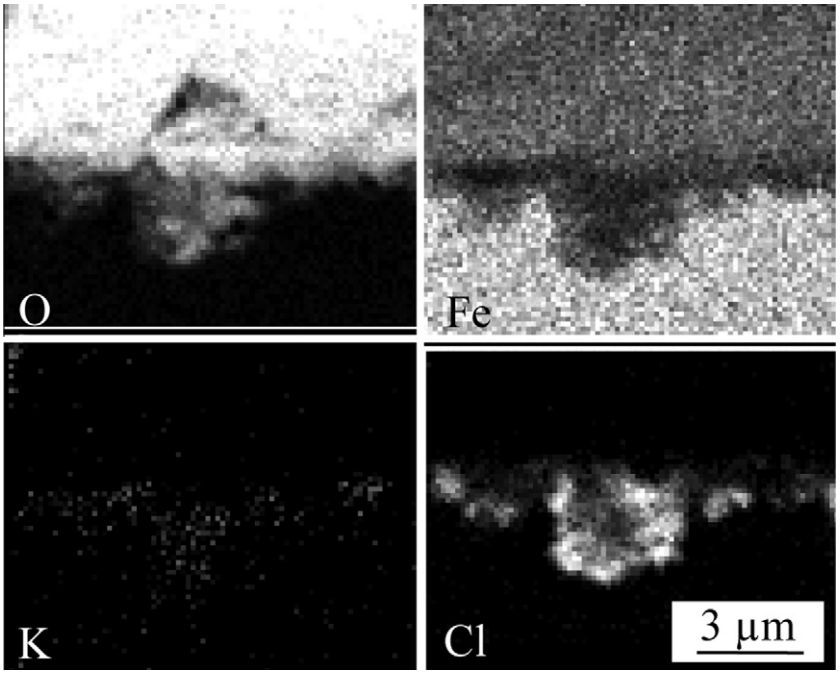

Fig. 4e. SEM/EDX maps of the cross-section shown in Fig. 4d. The inward growing part contains Cl together with O and Fe while the outward growing part mainly consists of an iron rich oxide.

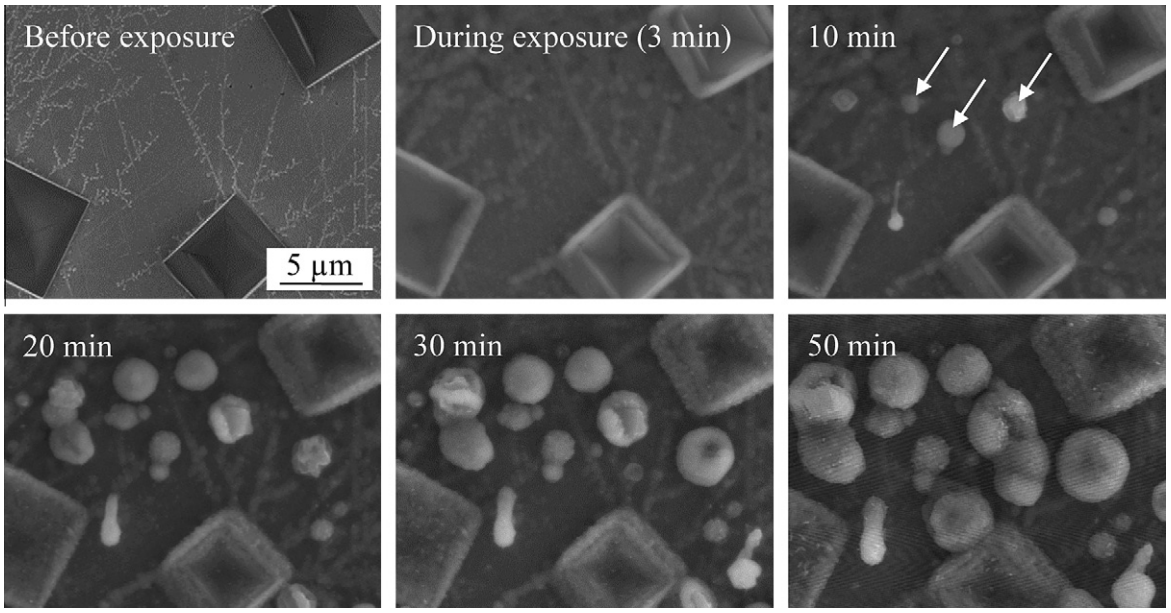

Fig. 5a. A thin dendritic network pattern of KCl region in between several KCl particles is shown before exposure and during the ESEM *in situ* exposure. Small oxide nodules which grow with exposure time can be seen after 10 min exposure (marked with arrows in the image). No large accumulation of KCl could be seen on these positions in the before image.

information about the structure. The dark 200–300 nm thick layer at the oxide/metal interface is mainly porous iron oxide, which contains some Cl (up to 5 at.%) together with low levels of Cr and Mo. The outer oxide is iron-rich (with <2 at.% of K and Cl). The outer iron-rich oxide and the accumulated KCl on top of the oxide nodules were also observed in plan view imaging and EDX analysis. The amount of KCl found at the top of the oxide nodules was not correlated to the amount of "dendritic" KCl present before exposure.

3.4. KCl particles on pre-oxidized steel

A number of samples were subjected to pre-oxidation (60 min at 400 °C) and subsequently prepared with KCl(s) and exposed *in situ* for 60 min at 400 °C. The distribution of KCl on the surface before the *in situ* experiment was the same as described above, featuring isolated KCl particles as well as KCl particles surrounded by small amounts of KCl dendrites (c.f. Fig. 1). Pre-oxidation resulted in the formation of a smooth 100–200 nm thick iron-rich oxide scale.

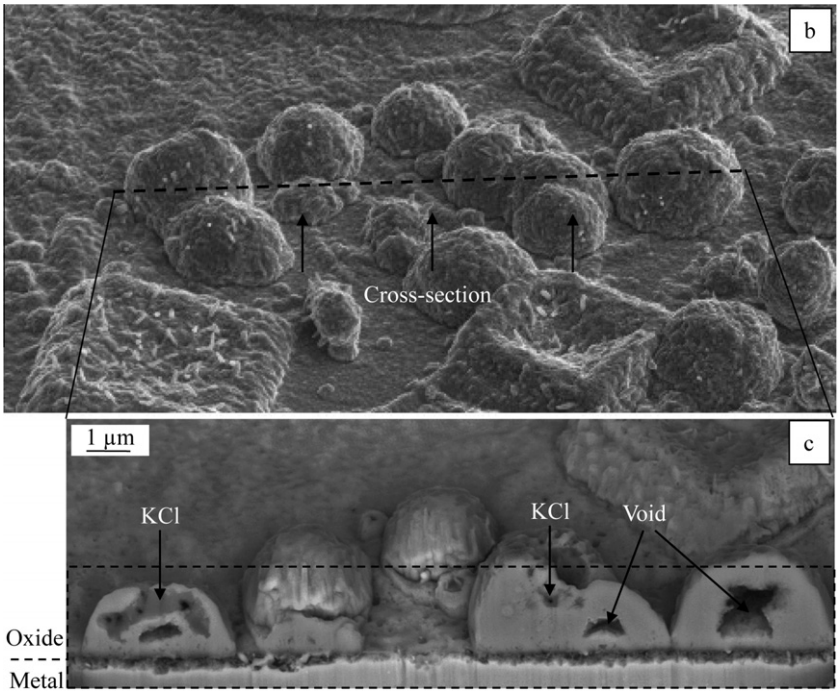

Fig. 5b and c. (b) An SE image after 60 min of exposure of the region shown in Fig. 5a. The sample is tilted 52° showing the corrosion products after several former KCl particles together with the rounded oxide nodules. The position of an ion-milled cross-section is marked in the image. (c) A BSE image of the ion-milled cross-section marked in (b). The cross-section was milled with 30° tilt to be able to acquire the subsequent SEM/EDX analysis. SEM/EDX maps of the marked area of the cross-section are shown in Fig. 5d.

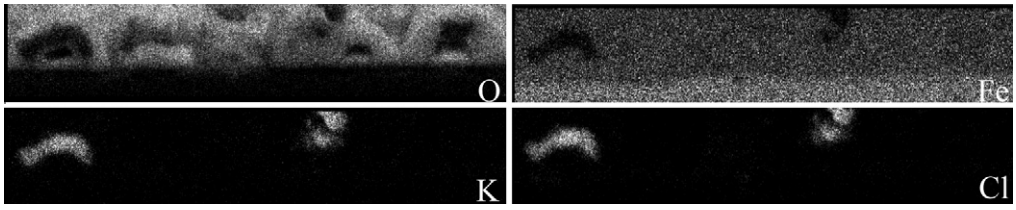

Fig. 5d. SEM/EDX maps of the marked region in the cross-section shown in Fig. 5c. KCl can be seen at the top of some of the round oxide nodules.

3.4.1. Isolated KCl particles (type a)

Fig. 6 shows a type a (isolated) KCl particle on a pre-oxidized sample before exposure, during *in situ* exposure (7 and 55 min) and after exposure. Exposure at 400 °C did not produce any sign of corrosion at or in the vicinity of the type a KCl particles. Thus, the surface morphology was hardly affected at all, and no oxide rim was formed.

3.4.2. KCl particles surrounded by KCl dendrites (type b)

In contrast to the type a KCl particles, the type b salt particles (surrounded by KCl dendrites) tended to become encircled by iron oxide (forming oxide rims) on the pre-oxidized samples. Fig. 7a shows a KCl particle surrounded with KCl dendrites before and during *in situ* exposure. An oxide rim is seen to form after 17 min and continues to grow throughout the exposure. The BSE image of an ion-milled cross-section through the KCl particle in Fig. 7b shows that the KCl particle is hollow. The oxide rim is about 2 µm thick and 1.5 µm wide. The oxide rim, the walls of the former KCl particle and the top part of the scale below the former KCl particle are all made up of iron oxide containing small amounts (<2.5 at.%) of K and Cl. The bottom part of the scale beneath the KCl appears dark in the image. EDX quantification showed that, in addition to iron and oxygen, this part of the scale contains small amounts of Cr and Mo but no Cl.

4. Discussion

4.1. General observations regarding the ESEM in situ exposure technique

In the present study the initial stages of the KCl-induced corrosion of Fe–2.25Cr–1Mo at 400 °C is investigated through ESEM *in situ* exposures and imaging. This technique provides a unique possibility to study high temperature corrosion as the microscope is operated at a higher pressure than a standard SEM and because the electron detector is not heat or light sensitive. A number of factors make ESEM *in situ* exposures different from standard furnace exposures. Thus, the sample is constantly irradiated with an electron beam and the pressure is lower than in an ordinary furnace exposure. Both these factors may affect the oxidation behaviour. However, a previous study has shown that exposure in the ESEM environment gives reproducible results and that the oxide scale microstructure observed on iron at 500 °C *in situ* in the ESEM (O_2 and $O_2 + H_2O$) is in excellent agreement with the oxide scale microstructure developed during corresponding well-controlled thermogravimetric exposures at atmospheric pressure [23]. The present results from *in situ* exposure in the ESEM without KCl are also in good agreement with corresponding furnace exposures concerning the composition, thickness and morphology of the scale.

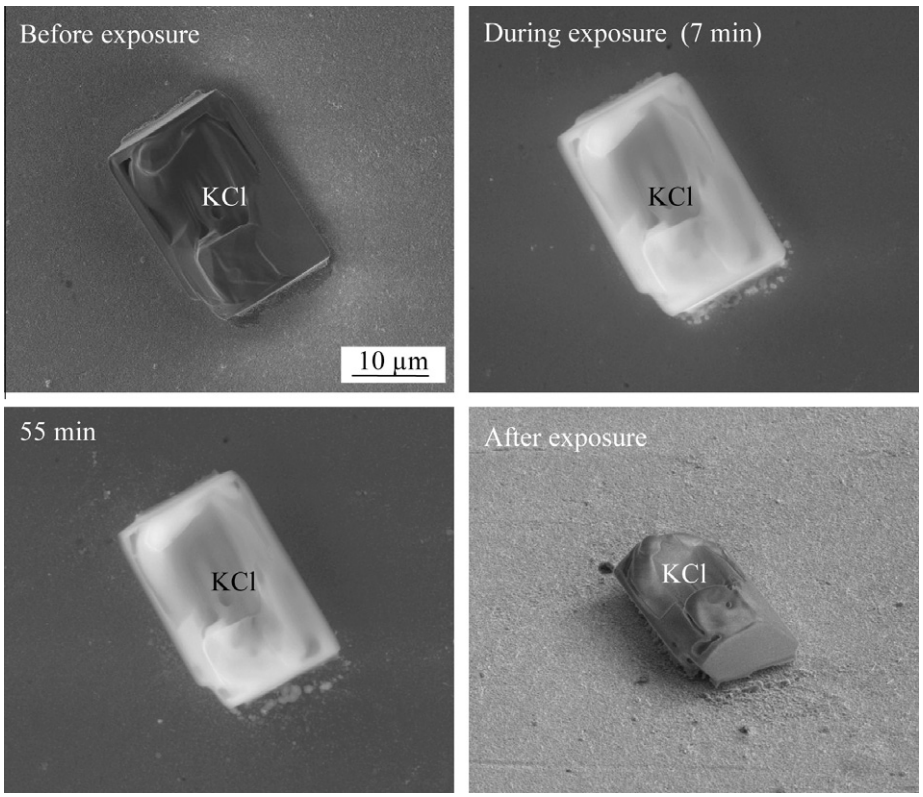

Fig. 6. An isolated KCl particle on a pre-oxidized sample (60 min at 400 °C) is shown before exposure and during ESEM *in situ* exposure at 400 °C and after exposure. The after exposure SE image shows the particle with 52° tilt. No oxide rim around the KCl particle could be seen growing with exposure time.

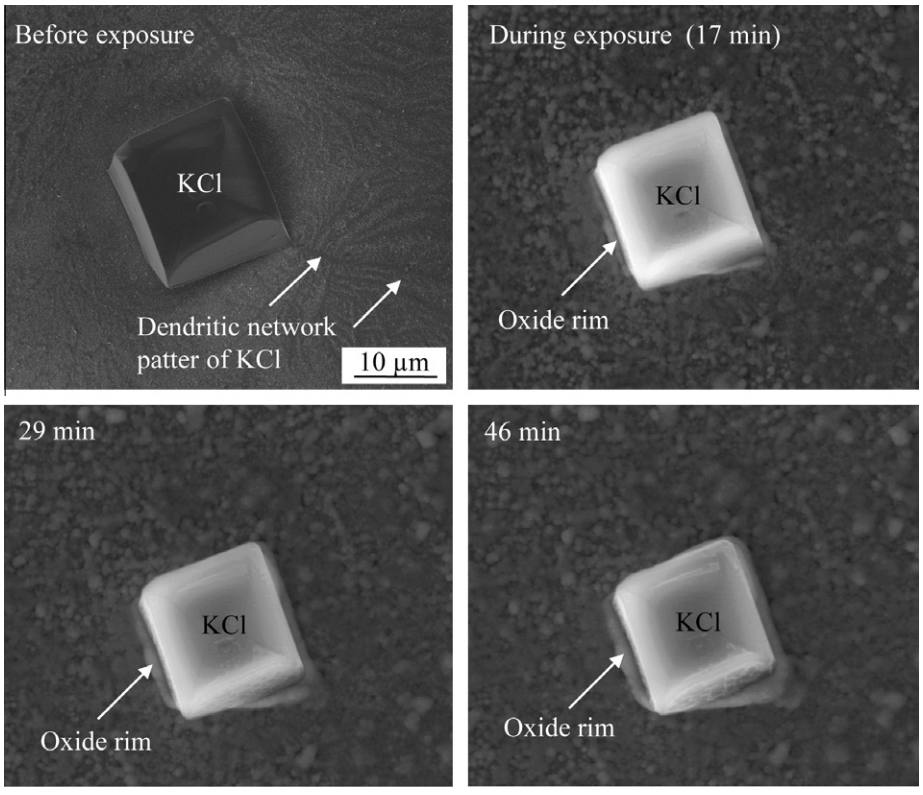

Fig. 7a. A KCl particle surrounded with a thin dendritic network pattern of KCl on a pre-oxidized sample (60 min at 400 °C) is shown before exposure and during the ESEM *in situ* exposure at 400 °C. An oxide rim around the KCl particle appears after 17 min exposure. The oxide rim grows with exposure time. An ion-milled cross-section through the particle is shown in Fig. 7b.

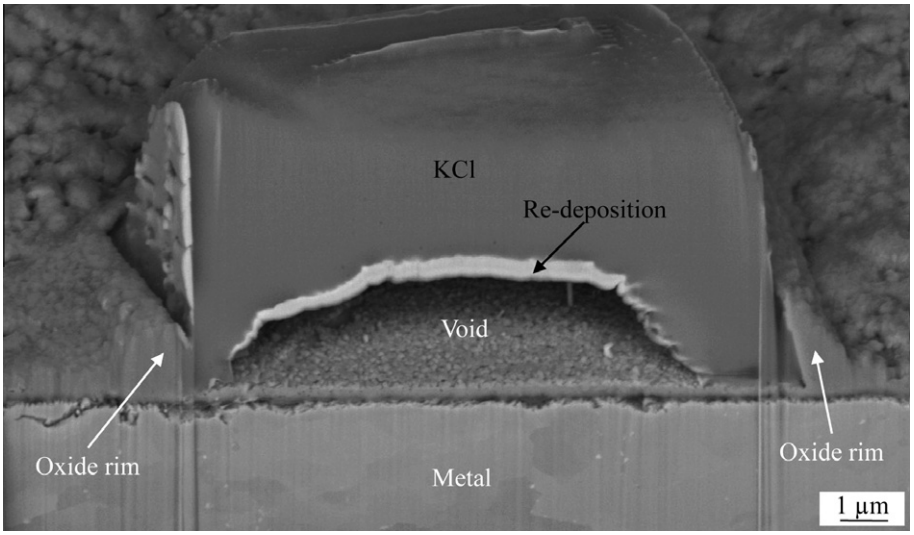

Fig. 7b. A SEM/BSE image of an ion-milled cross-section through the KCl particle shown in Fig. 7a. The cross-section was milled with 45° tilt in order to be able to perform the subsequent SEM/EDX analysis. The oxide rim around the KCl particle and a micrometer thick oxide scale beneath it can be seen. The cross-section reveals that the KCl particle is hollow.

While there was no indication that the electron beam had any effect on the KCl crystallites, the lower pressure did cause a higher evaporation rate compared to furnace exposures. However, as evaporation was still rather slow it is considered that this effect did not influence the results. Moreover, all the different morphological features found after 1 h's exposure in the ESEM were also observed after 1 h's exposure in a furnace at atmospheric pressure, see [19]. In fact the surface morphologies are very similar and differences between the two types of exposures are insignificant compared to the local variations on individual samples.

4.2. Oxidation without KCl

It is well known that oxidation of iron in oxygen-containing gases at 400 °C results in the formation of a relatively thin hematite top layer and a thicker bottom magnetite layer [2]. Several recent investigations of iron oxidation in this temperature range show that the magnetite layer actually consists of a lower inward-growing part and an outer outward growing part [23,25–31]. A study of the oxidation behaviour of a binary Fe–2.25Cr steel at 600 °C [32] showed a similar three-layered scale structure. In that case, the bottom inward-growing layer was reported to consist of iron chromium spinel oxide while the chromium free upper part of the scale was made up of a middle magnetite layer and a hematite layer on top. The fact that chromium was only present in the inner layer was explained by the comparatively slow diffusion of Cr^{3+} in spinel oxide [33]. The scale thickness and morphology observed in the present study on Fe–2.25Cr–1Mo steel at 400 °C in the absence of KCl is in good agreement with these earlier studies, Fe–2.25Cr–1Mo forming a slow growing scale at 400 °C. The resolution of the FIB imaging is not sufficient in order to divide the scale into an outward growing and an inward growing part after 1 h's exposure at 400 °C.

4.3. The influence of KCl on the initial oxidation

This study illustrates the strongly corrosive nature of KCl towards Fe–2.25Cr–1Mo steel at 400 °C. Thus, the base oxide is thicker (about 500 nm, see Fig. 3b) than in the corresponding exposure without KCl (about 100–200 nm). Moreover, large parts of the sample surface become covered by thick corrosion products after only 1 h's exposure while in the absence of KCl the corresponding exposure produced a very thin oxide scale. This is in good agreement with a previous study of KCl-induced corrosion of low alloy steel using conventional furnace exposures [19]. The present ESEM *in situ* study highlights the great local variations in corrosion kinetics and corrosion product morphology, emphasizing the importance of the initial distribution of KCl on the surface.

The rapidity of the corrosion attack, especially in the vicinity of type b salt particles (surrounded by KCl dendrites) is a prominent feature of this study. Thus, the reaction starts within the first minutes of exposure at 400 °C or even during temperature ramping, see Figs. 3a and b and 4a–d. The rapid overgrowing of the KCl crystals by iron oxide (Fig. 4b), the consumption of the KCl particles and the occurrence of new KCl aggregates in the spherical corrosion products that form around the type b KCl particles is remarkable (see Fig. 4b), showing that both iron ions and potassium ions are transported very rapidly on the surface. Similar agglomerations of oxide on and in the vicinity of KCl particles have been reported in investigations of the KCl-induced corrosion of stainless steels [16–18]. The phenomenon was attributed to the interaction of $FeCl_2$ and KCl, resulting in the formation of highly mobile iron chloride species on the surface [18].

The rapid lateral transport observed in the present case implies the presence of a liquid phase on the surface. It is considered that the most probable candidate for such melt formation is the $FeCl_2$/KCl system [34]. The following corrosion reaction is suggested to account for the formation of $FeCl_2$:

$$(\text{scale/gas interfaces})\ 2KCl(s) + 1/2O_2 + H_2O + 2e^- \rightarrow 2KOH(ads) + 2Cl^-(ads) \quad (1)$$

$$(\text{scale/metal interface})\qquad Fe \rightarrow Fe^{2+} + 2e^- \quad (2)$$

Thus, the formation of chloride ions on the scale surface is coupled to the formation of iron ions at the scale/substrate interface by electronic conduction and ionic conduction (grain boundary) through the oxide scale.

It may be noted that the reaction scheme involves the exchange of K^+ for Fe^{2+} as counterion to Cl^-. To maintain charge neutrality potassium must therefore receive another counterion, either the hydroxide ion or (in the absence of water vapour) the oxide ion. This means that the scale surface becomes alkaline, corresponding to a high activity of KOH (or K_2O). The KOH can then either

volatilize and leave the surface or react with iron oxide to form potassium ferrate(III). Volatilization of KOH is expected to be significant because of its relatively high vapour pressure at 400 °C and because the experiment is performed at a reduced pressure (2.5 Torr). The apparent equilibrium partial pressure of KOH ($p(tot)KOH = pKOH + 2p(KOH)_2$) at 400 °C was estimated to be in the range $2–8 \times 10–7$ atm by extrapolating the data of Konings and Cordfunke [35]. The sum (cell) reaction then becomes:

$$2KCl(s) + 1/2O_2 + H_2O + Fe \rightarrow 2KOH(g) + FeCl_2 \quad (3)$$

Alternatively, the KOH formed on the scale surface may react with iron oxide forming potassium ferrate:

$$2KOH(ads) + Fe_2O_3(s) \leftrightarrow 2KFeO_2(s) + H_2O(g) \quad (4)$$

In this scheme, iron chloride is expected to form where chloride and iron ions encounter each other. Thus, in order to form $FeCl_2$ on the scale surface, the transport of iron ions through the scale has to be comparatively fast. After exposure, chlorine was frequently found at the metal/oxide interface, while the outward growing part of the scale consisted of iron oxide with no chlorine. The distribution of iron chloride after exposure is attributed to the fact that iron chloride is thermodynamically stable in the sub scale region while it is unstable in the more oxidizing conditions in the top parts of the scale. Chromium was only found in the inner part of the oxide scale, which is in good agreement with the predictions of chromium diffusivity in the spinel described above.

The observation of iron chloride in the bottom part of the scale after exposure (Fig. 4d) implies that the formation of iron chloride occurs at the bottom of the scale as well as on the scale surface. The accumulations of iron chloride at the scale substrate interface is expected to decrease the adhesion of the oxide scale and spallation was indeed observed on several samples, see Fig. 3b.

It is considered that the formation of a thin $FeCl_2$/KCl liquid film on the scale surface can explain several of the observations in this study. The presence of $FeCl_2$ at the scale/gas interface appears to be at odds with thermodynamic stability of $FeCl_2$. However, metastable phases are often observed in corrosion experiments, especially at "moderate" temperatures as in the present case. Moreover, $FeCl_2$ was reported to form at the scale/gas interface on stainless steel in an oxidizing environment [36]. Thus, the presence of a $FeCl_2$/KCl liquid film together with the KCl crystals sets up concentration gradients on the surface that will cause iron chloride to diffuse towards the original KCl crystals while KCl will diffuse away from the original KCl crystals. Iron chloride is thermodynamically unstable at the scale/gas interface and tends to decompose into iron oxide + HCl e.g.:

$$2FeCl_2 + 1/2O_2(g) + 2H_2O(g) \rightarrow Fe_2O_3(s) + 4HCl(g) \quad (5)$$

Thus, the agglomeration of iron oxide in the vicinity of type b KCl crystals is attributed to the combined effects of lateral iron chloride diffusion on the surface and iron chloride decomposing into iron oxide. The observation that the accumulation of iron oxide at type b KCl crystals starts at about 355 °C (Fig. 4b) lends further support to the crucial role played by the KCl/$FeCl_2$ system as this corresponds to the eutectic temperature in that system [34].

Consequently, it is argued that the initial reaction in the area between the type b salt particles involves iron chloride formation (reactions 1, 2 and 3 or 4), the small amounts of dendritic salt particles providing the KCl necessary for the reaction. Part of the iron chloride will form at the scale surface, creating a thin liquid film together with un-reacted KCl. Because of the concentration gradients in the thin liquid film, its iron chloride component diffuses towards the type b KCl particles. Simultaneously, and driven by the same concentration gradient, KCl diffuses in the opposite direction, away from the type b particles to the region between the particles. This allows the reaction (1, 2, 3 or 4) to continue on the surface. In the absence of such transport the small amount of KCl present between the type b particles would soon be consumed and the reaction would cease.

The corrosion morphology observed between type b particles (Figs. 5a–c) featuring roughly hemispherical corrosion product agglomerations with KCl inclusions is characteristic. The observation that these agglomerations are not connected to preferential attack of the substrate implies rapid lateral transport of iron ions on the surface and that their formation is analogous to the formation of the iron oxide agglomerates at the former type b KCl particles. Thus, it is proposed that the "nucleation" of the spherical agglomerates corresponds to a local decomposition of the $FeCl_2$ component of the KCl/$FeCl_2$ eutectic film, resulting in the formation of iron oxide and solid KCl. While part of the KCl produced in this way will continue to be involved in the corrosion process (1, 2, 3 or 4), it is proposed that another part of the KCl, forming at locations where the resistance in the electrochemical cell (1, 2, 3 or 4) is high (i.e. where the oxide is protective and/or thick), is not consumed. These electrochemically inactive KCl agglomerations will set up radial concentration gradients around them, resulting in the transport of iron chloride towards them, explaining the continued accumulation of iron oxide throughout the exposure. With time, as the KCl is eventually consumed, either by reaction with the substrate or by vaporization, the growth of the hemispherical iron oxide agglomerations must cease.

The corrosion reaction in the vicinity of type a KCl particles is markedly slower compared to the type b case and no formation of spherical oxide agglomerations is observed. The formation of an oxide rim around the KCl particles and the rapid consumption of KCl nevertheless imply that the reaction is basically the same as in the type b case. The relative slowness of the reaction is attributed to the relative scarcity of KCl on the surface. Hence, lack of hemispherical oxide nodules suggests that the KCl released by decomposition of the $FeCl_2$/KCl eutectic is all consumed in the corrosion reaction (1, 2, 3 or 4).

As expected, pre-oxidized steel reacts much more slowly in the presence of KCl (see Figs. 6 and 7). Thus, the rate of corrosion attack and corrosion morphology close to type b KCl particles on pre-oxidized steel is similar to that of type a KCl particles on "virgin" steel (compare Figs. 3b and 7b). Moreover, there is little evidence for any corrosion attack around the type a particles on pre-oxidized steel. The slowness of the reaction is attributed to the presence of a relatively thick and protective iron oxide scale, which has low transport rates for ionic species. This corresponds to a high resistance in the electrochemical cell (reactions (1, 2, 3 or 4)) and a slow corrosion rate.

The present study shows that, as a result of the initial formation of a KCl/$FeCl_2$ film on the oxide surface, KCl becomes distributed over the whole surface, causing general corrosion of the steel. This is in accordance with a furnace study involving longer exposure times [19] where the presence of low levels of KCl on a Fe–2.25Cr–1Mo steel was reported to result in a thick multilayer scale covering the whole sample after 168 h exposure at 400 °C. The presence of KCl causes the base oxide to be thicker compared to the reference case indicating a faster ionic transport through the scale. Also, Cl was found at the metal/oxide interface, showing that Cl is transported through the scale, presumably by grain boundary transport of chloride. This is supported by previous studies of chloride-induced corrosion of steel [19,36]. We find that the initial distribution of KCl is important since the formation of $FeCl_2$/KCl eutectic film only occurs when the oxide scale is thin. Thus, we observe that areas where small amounts of KCl are present between the KCl particles (type b) are exposed to a larger amount of Cl, generating a higher corrosion rate.

5. Conclusions

The present study demonstrates the strongly corrosive nature of KCl towards the low alloyed steel Fe–2.25Cr–1Mo at 400 °C. Several characteristic features of the oxide scale morphology and microstructure have been observed through a combination of experimental techniques.

- The corrosion reaction starts well below 400 °C and results in a rapid redistribution of KCl and iron ions over the surface. Thus, iron oxide agglomerates at the location of the former KCl particles forming oxide "rims" and "shells". Also, while the KCl particles present at the start of the experiment are rapidly consumed, new KCl agglomerations appear on the scale surface.
- The rapid lateral transport of KCl and corrosion products on the surface is attributed to the formation of a thin liquid film consisting of a KCl/$FeCl_2$ mixture (eutectic temperature = 355 °C); concentration gradients in the film provides the driving force for the surface diffusion of $FeCl_2$ and KCl. With time, $FeCl_2$ on the surface decomposes into iron oxide and HCl.
- The KCl induced corrosion of low alloy steel in air at 400 °C is initiated by the reaction of KCl with O_2 and H_2O at the gas/oxide interface, forming KOH and/or $KFeO_2$ together with chloride ions. This surface reaction is coupled to the oxidation of Fe to Fe^{2+} at the scale/metal interface by electronic and ionic currents through the oxide.
- Pre-oxidation of the steel slows down the process considerably. This is attributed to a greater resistance to Fe^{2+} and Cl^- transport.
- Increased oxidation rate was observed all over the sample. This is attributed to an increased diffusion rate through the scale caused by the presence of Cl^- at oxide grain boundaries.
- ESEM *in situ* exposures and analysis are very powerful tools for the study of KCl induced high temperature corrosion, especially if combined with low voltage imaging prior to exposure and FIB milling and imaging afterwards.

Acknowledgements

This work was carried out within the Swedish High Temperature Corrosion centre (HTC). A grant from the Knut and Alice Wallenberg Foundation for acquiring the FEG SEM instrument is gratefully acknowledged.

References

[1] P. Kofstad, High Temperature Corrosion, Elsevier Applied Science Publishers Ltd., London and New York, 1988.
[2] N. Birks, H. Meier, Introduction to the High Temperature Oxidation of Metals, second ed., Cambridge University Press, London, 2006.
[3] L.-G. Johansson, J.-E. Svensson, E. Skog, J. Pettersson, C. Pettersson, N. Folkeson, H. Asteman, T. Jonsson, M. Halvarsson, Critical corrosion phenomena on superheaters in biomass and waste-fired boilers, Journal of Iron and Steel Research International 14 (2007) 35–39.
[4] T. Jonsson, J. Pettersson, K. Davidsson, L.-G. Johansson, J.-E. Svensson, Sewage sludge as additive to reduce the initial fireside corrosion caused by combustion of shredder residues in a waste-fired BFB boiler, in: Ninth Liège Conference on Materials for Advanced Power Engineering, Liege, 2010.
[5] H.P. Nielsen, The Implications of Chlorine-associated Corrosion on the Operation of Biomass-fired Boilers, Progress in Energy and Combustion Science 26 (2000) 283–298.
[6] J.-M. Abels, H.-H. Strehblow, A surface analytical approach to the high temperature chlorination behaviour of inconel 600 at 700 °C, Corrosion Science 39 (1997) 115–132.
[7] S.C. Cha, M. Spiegel, Local reactions of KCl particles with iron, nickel and chromium surfaces, Materials and Corrosion 57 (2006) 159–164.
[8] H.J. Grabke, E. Reese, M. Spiegel, The effects of chlorides, hydrogen-chloride, and sulfur-dioxide in the oxidation of steels below deposits, Corrosion Science 37 (1995) 1023–1043.
[9] M.J. McNallan, W.W. Liang, S.H. Kim, C.T. Kang, Acceleration of the high temperature oxidation of metals by chlorine, high temperature corrosion, NACE (1983) 316–321.
[10] A. Zahs, M. Spiegel, H.J. Grabke, The influence of alloying elements on the chlorine-induced high temperature corrosion of Fe–Cr alloys in oxidizing atmospheres, Materials and Corrosion 50 (1999) 561–578.
[11] A. Zahs, M. Spiegel, H.J. Grabke, Chloridation and oxidation of iron, chromium, nickel and their alloys in chloridizing and oxidizing atmospheres at 400–700 °C, Corrosion Science 42 (2000) 1093–1122.
[12] Y.S. Li, Y. Niu, W.T. Wu, Accelerated corrosion of pure Fe, Ni, Cr and several Fe-based alloys induced by $ZnCl_2$–KCl at 450 °C in oxidizing environment, Materials Science and Engineering, A: Structural Materials: Properties, Microstructure and Processing 345 (2003) 64–71.
[13] C. Pettersson, J. Pettersson, H. Asteman, J.-E. Svensson, L.-G. Johansson, KCl-induced high temperature corrosion of the austenitic Fe–Cr–Ni alloys 304L and Sanicro 28 at 600 °C, Corrosion Science 48 (2005) 1368–1378.
[14] C. Pettersson, L.G. Johansson, J.E. Svensson, The influence of small amounts of KCl(s) on initial stages of the corrosion of alloy Sanicro 28 at 600 °C, Oxidation of Metals 70 (2008) 241–256.
[15] J. Pettersson, J.E. Svensson, L.G. Johansson, Alkali induced corrosion of 304-type austenitic stainless steel at 600 °C; comparison between KCl, K_2CO_3 and K_2SO_4, in: P. Steinmetz, I.G. Wright, A. Galerie, D. Monceau, S. Mathieu (Eds.), Seventh International Symposium on High Temperature Corrosion and Protection of Materials, Les Embiez, France, 2008, pp. 367–375.
[16] T. Jonsson, J. Froitzheim, J. Pettersson, J.-E. Svensson, L.-G. Johansson, M. Halvarsson, The influence of KCl on the corrosion of an austenitic stainless steel (304L) in oxidizing humid conditions at 600 °C: a microstructural study, Oxidation of Metals 72 (2009) 213–239.
[17] T. Jonsson, J. Froitzheim, J. Pettersson, J.-E. Svensson, L.-G. Johansson, M. Halvarsson, Microstructural investigation of the influence of KCl on the corrosion of 304L exposed to 5% $O_2 + N_2$, in: 16th International Corrosion Congress, Beijing, China, 2005.
[18] C. Proff, T. Jonsson, C. Pettersson, J.-E. Svensson, L.-G. Johansson, M. Halvarsson, Microstructural investigation of the KCl-induced corrosion of the austenitic alloy Sanicro 28 (35Fe27Cr31Ni) at 600 °C, Materials at High Temperature 26 (2009) 113–125.
[19] N. Folkeson, T. Jonsson, M. Halvarsson, L.-G. Johansson, J.-E. Svensson, The influence of small amounts of KCl(s) on the high temperature corrosion of a Fe–2.25Cr–1Mo steel at 400 and 500 °C, Materials and Corrosion, n/a, doi:10.1002/maco.201005942.
[20] B. Pöter, I. Parezanovic, M. Spiegel, In situ scanning electron microscopy and electron backscatter diffraction investigation on the oxidation of pure iron, Materials at High Temperature 22 (2005) 9–17.
[21] B. Schmid, N. Aas, O. Grong, R. Odegård, High-temperature oxidation of iron and the decay of Wüstite studied with in situ ESEM, Oxidation of Metals 57 (2002) 115–130.
[22] P. Bruckel, P. Lours, P. Lamesie, B. Pieraggi, In situ ESEM investigations of the oxide growth on hot work tools: effect of the water vapour, Materials at High Temperature 20 (2003) 551–560.
[23] T. Jonsson, B. Pujilaksono, S. Hallström, J. Ågren, J.-E. Svensson, L.-G. Johansson, M. Halvarsson, An ESEM in situ investigation of the influence of H_2O on iron oxidation at 500 °C, Corrosion Science 51 (2009) 1914–1924.
[24] A. Järdnäs, J.-E. Svensson, L.-G. Johansson, Evidence for the suppression of the oxidation of a Fe 2.25Cr 1 Mo steel by traces of SO_2, Material Science Forum 369–372 (2001) 173–180.
[25] A. Atkinson, R.I. Taylor, A.E. Hughes, A quantitative demonstration of the grain-boundary diffusion mechanism for the oxidation of metals, Philosophical Magazine A: Physics of Condensed Matter. Structure Defects and Mechanical Properties 45 (1982) 823–833.
[26] R.Y. Chen, W.Y.D. Yuen, Review of the high-temperature oxidation of iron and carbon steels in air or oxygen, Oxidation of Metals 59 (2003) 433–468.
[27] C. Gleave, J.M. Calvert, D.G. Lees, P.C. Rowlands, A study of the mechanism of corrosion of some ferritic steels in high-pressure carbon dioxide with the aid of oxygen-18 as a tracer. II. High-silicon mild steel, in: R. Soc. Mathematical, Physical and Engineering Sciences, London, 1982, pp. 429–438.
[28] T. Jonsson, A. Järdnäs, J.-E. Svensson, L.-G. Johansson, M. Halvarsson, The effect of traces of SO_2 on iron oxidation: a microstructural study, Oxidation of Metals 67 (2007) 193–213.
[29] M. Ueda, K. Kawamura, T. Maruyama, Void formation in magnetite scale formed on iron at 823 K – elucidation by chemical potential distribution, High-Temperature Oxidation and Corrosion (2005) 37–44.
[30] N. Bertrand, C. Desgranges, D. Gauvain, D. Monceau, D. Poquillon, p. trans tech, Low temperature oxidation of pure iron: growth kinetics and scale morphologies, in: P. Steinmetz, I.G. Wright, G. Meier, A. Galerie, B. Pieraggi, R. Podor (Eds.), High Temperature Corrosion and Protection of Materials 6, Prt 1 and 2, Proceedings, Trans Tech Publications Ltd., Zurich-Uetikon, 2004, pp. 591–598.
[31] B. Pujilaksono, T. Jonsson, M. Halvarsson, J.-E. Svensson, L.-G. Johansson, Oxidation of iron at 400–600 °C in dry and wet O_2, Corrosion Science 52 (2010) 1560–1569.
[32] B. Pujilaksono, T. Jonsson, H. Heidari, M. Halvarsson, J.-E. Svensson, L.-G. Johansson, Oxidation of binary FeCr alloys (Fe–2.25Cr, Fe–10Cr, Fe–18Cr and Fe–25Cr) in O_2 and in $O_2 + H_2O$ environment at 600 °C, Oxidation of Metals 75 (2011) 183–207.
[33] J. Topfer, S. Aggarwal, R. Dieckmann, Point-defects and cation tracer diffusion in (CRXFE1-X)(3-DELTA)O-4 spinels, Solid State Ionics 81 (1995) 251–266.

[34] E.M. Levin, C.R. Robbins, H.F. McMurdie, Phase Diagrams for Ceramists, The American Ceramic Society, 1964.
[35] R.J.M. Konings, E.H.P. Cordfunke, The vapor-pressures of hydroxides. 1. The alkali hydroxides KOH and CSOH, Journal of Chemical Thermodynamics 20 (1988) 103–108.
[36] N. Folkeson, L.G. Johansson, J.E. Svensson, Initial stages of the HCl-induced high-temperature corrosion of alloy 310, Journal of the Electrochemical Society 154 (2007) C515–C521.